Journal of Controlled Release 390 (2026) 114518

Contents lists available at ScienceDirect

Journal of Controlled Release

journal homepage: www.elsevier.com/locate/jconrel

Phosphatase and tensin homolog mRNA complexed with hyaluronated lipid nanoparticles for transdermal cancer immunotherapy

Mungu Kim, Zhengyu Piao, Jin Huh *, Sei Kwang Hahn *

Department of Materials Science and Engineering, Pohang University of Science and Technology (POSTECH), 77 Cheongam-ro, Nam-gu, Pohang, Gyeongbuk 37673, Republic of Korea

ARTICLE INFO

Keywords:
Hyaluronate
Targeted lipid nanoparticle
mRNA
Phosphatase and tensin homolog
Skin cancer immunotherapy
Transdermal cancer immunotherapy

ABSTRACT

The loss of phosphatase and tensin homolog (PTEN) can lead to resistance to immune checkpoint inhibitors (ICIs) in melanoma, thereby promoting immune evasion and tumor progression. These effects can be reversed by restoring PTEN expression, reactivating antitumor immunity, and enhancing therapeutic responses. Here, we develop a hyaluronate-conjugated lipid nanoparticle (HA-LNP) with HA-dimyristoyl glycerol (DMG) for the non-invasive, transdermal delivery of PTEN mRNA. This amphiphilic lipid enables stable HA integration during LNP self-assembly, effectively replacing PEG, supporting particle stability, biocompatibility, and CD44-mediated targeting. The resulting HA-LNP efficiently encapsulate large mRNA payloads, penetrate the skin, and selectively target CD44-expressing tumor cells. *In vitro*, PTEN mRNA@HA-LNP restores PTEN expression, induces immunogenic cell death (ICD), and reduces melanoma cell viability. *In vivo*, topical application results in deep skin and tumor penetration, significantly inhibiting tumor growth and enhancing immune activation with minimal toxicity. Taken together, these results highlight HA-LNP as a promising, clinically translatable platform for localized, mRNA-based cancer immunotherapy.

1. Introduction

Melanoma is the most aggressive form of skin cancer, arising from the uncontrolled proliferation of melanocytes [1,2]. Melanoma is particularly challenging to treat due to its high metastatic potential, late-stage diagnosis, and limited curative capacity of surgical resection [3]. Although immune checkpoint inhibitors (ICIs), such as anti-PD-1 and anti-CTLA-4, have transformed melanoma treatment, fewer than 50 % of patients experience sustained clinical benefit, with the frequent development of tumor resistance [4–6]. One such tumor suppressor, phosphatase and tensin homolog (PTEN), plays a crucial role in regulating cell proliferation, survival, and metabolism by inhibiting the PI3K/AKT signaling pathway [7,8]. PTEN loss or mutation is commonly observed in various malignancies, including glioblastoma [9], breast cancer [10], prostate cancer [11], and melanoma [12], where it contributes to unchecked cell growth, reduced apoptosis, and enhanced metastatic behavior. The loss of PTEN impairs T cell infiltration and cytotoxic activity, promoting immune evasion and resistance to ICIs [13–15].

Restoring PTEN expression has been shown to suppress tumor progression, sensitize tumors to chemotherapy, and re-engage immune-mediated tumor clearance. Efforts to restore PTEN expression have included gene-replacement strategies using DNA vectors, viral delivery systems, and recombinant proteins. However, these approaches face limitations, including risks of genomic integration, immunogenicity, and poor cytosolic delivery [16]. In contrast, mRNA-based therapeutics offer a non-integrating, transient, and tunable alternative that enables direct cytoplasmic expression of therapeutic proteins [17–19]. Chemically modified mRNA can be rapidly designed for enhanced stability and translation, making it an attractive platform for delivering PTEN to tumor cells with minimal off-target effects and immunological risks [20]. Lipid nanoparticles (LNPs) have emerged as clinically validated vehicles for mRNA delivery and have been adapted for transdermal applications *via* the surface modification with hyaluronate (HA) [21–23]. HA is a biocompatible glycosaminoglycan that facilitates skin penetration *via* CD44 receptor-mediated uptake, hydration effects, and interactions with structural skin proteins [24–26]. The skin has abundant CD44-expressing cells, including antigen-presenting cells (APCs), keratinocytes, and fibroblasts, making it an ideal site for HA-targeted delivery [27,28].

In this work, we develop a notable class of HA-conjugated LNP (HA-LNP) incorporating HA-DMG as a scalable lipid conjugate. HA-DMG is designed to integrate directly into the lipid bilayer during LNP self-

* Corresponding authors.
E-mail addresses: jinhuh@postech.ac.kr (J. Huh), skhanb@postech.ac.kr (S.K. Hahn).

https://doi.org/10.1016/j.jconrel.2025.114518
Received 1 August 2025; Received in revised form 26 November 2025; Accepted 6 December 2025
Available online 11 December 2025

assembly, eliminating the need for the post-formulation with HA surface coating. Poly(ethylene glycol) (PEG)-conjugated lipids are known to be the possible cause of anaphylaxis with immunogenicity [29]. Instead of the PEG-lipid, HA-DMG functions as both a stabilizing component and a targeting ligand, thereby enhancing particle uniformity and colloidal stability. Its amphiphilic structure ensures stable incorporation into the LNP core, displaying HA moieties on the surface to facilitate skin penetration and CD44-mediated targeting of tumor cells [30]. Compared to conventional PEG-LNPs, our HA-LNP exhibit superior skin penetration, enhanced uptake by CD44-positive tumor cells, and improved biocompatibility in a melanoma mouse model. The transdermal delivery of PTEN mRNA using HA-LNP induces immunogenic cell death (ICD), triggers the release of damage-associated molecular patterns (DAMPs), and suppresses the growth of melanoma. We assessed HA-LNP as a promising, scalable platform for non-invasive, tumor-targeted mRNA immunotherapy.

2. Materials and methods

2.1. Materials

P-toluenesulfonyl chloride (TsCl), triethylamine (TEA), 4-dimethylaminopyridine (DMAP), dichloromethane (DCM), ether, and sodium borate were purchased from Daejeong (Seoul, Korea). Ethanol, sodium cyanoborohydride, diaminobutane (DAB), 40 % tetrabutylammonium hydroxide (TBA), Triton X-100, cholesterol, 1-ethyl-3-[3-(dimethylamino)propyl]carbodiimide hydrochloride (EDC), N-hydroxysuccinimide sodium salt (NHS), and Amicon ultra centrifugal filter units were obtained from Sigma-Aldrich (St. Louis, MO). 1,2-Dimyristoyl-rac-glycerol (DMG) was purchased from GoldBio (St. Louis, MO). 1,2-DMG-3-methoxypolyethylene glycol 2000 (DMG-PEG) and 1,2-distearoyl-sn-glycero-3-phosphocholine (DSPC) were purchased from Avanti Polar Lipids (Alabaster, AL). 4′,6-Diamidino-2-phenylindole (DAPI) was purchased from Abcam (Cambridge, UK) and 8-[(2-hydroxyethyl)[6-oxo-6-(undecyloxy)hexyl]amino]octanoic acid (SM-102) was purchased from Cayman Chemical (Ann Arbor, MI). CleanCap EGFP mRNA was purchased from Trilink BioTechnologies (San Diego, CA). EZ Cap Cy5 EGFP mRNA and human PTEN mRNA were purchased from ApexBio Technology (Houston, TX). Lipofectamine MessengerMAX mRNA transfection reagent and Pierce™ BCA Protein assay kit were purchased from Thermo Fisher Scientific (Waltham, MA). Sodium hyaluronate (HA) was obtained from Lifecore Co. (Chaska, MN). Phosphate-buffered saline (PBS, pH 7.4), 10× TBS solution, lysis buffer and sodium acetate buffer solution (pH 4.5) were purchased from T&I (Chuncheon, Korea). The Cell Counting Kit-8 (CCK-8) and EZ-ATP Assay Kit were obtained from DoGenBio (Seoul, Korea). The mouse melanoma cell line (B16F10) was obtained from the Korean Cell Line Bank (Seoul, Korea). Cells were cultured in Dulbecco's modified Eagle's medium (DMEM) (Gibco, Waltham, MA) supplemented with fetal bovine serum (FBS) (T&I, Chuncheon, Korea) and penicillin/streptomycin (Corning, Corning, NY). Confocal dishes and culture flasks were obtained from SPL (Pocheon, Korea). Culture plates were purchased from Corning (Corning, Corning, NY). Quant-it™ RiboGreen reagent and RNA assay kit, tissue extraction reagent I, and TNF-α ELISA kit were purchased from Invitrogen (Waltham, MA). A cytotoxicity assay was performed using EZ-Cytox (DoGenBio, Seoul, Korea). Xpert Duo inhibitor cocktail solution was obtained from Gendepot (Baker, TX). The HMGB-1 ELISA kit was purchased from Abebio (Wuhan, China). TUNEL assay kit and goat anti-mouse secondary antibody (ab205719) were purchased from Abcam (Cambridge, UK). PTEN polyclonal antibody (51–2400) and goat anti-rabbit secondary antibody (31460) were purchased from Invitrogen (Waltham, MA). β-Actin antibody (sc-69879) was purchased from Santa Cruz Biotechnology (Dallas, TX).

2.2. Synthesis and characterization of HA-DMG

To synthesize HA-DAB-TBA, 5 kDa HA was dissolved in sodium borate buffer (pH 8.5) and mixed with DAB at a molar ratio of 15, along with sodium cyanoborohydride at a molar ratio of 5. The solution was stirred at 40 °C for 3 days. After the reaction, the mixture was concentrated by evaporation, then placed in a dialysis tube containing 0.1 M HCl, and then transferred to distilled water. To synthesize Tosyl-DMG, DMG, TsCl, and TEA were added in an equal molar ratio to DCM, along with DMAP at a molar ratio of 0.5. After introducing nitrogen gas, the mixture was stirred at room temperature for 4 h. HA-DAB-TBA and Tosyl-DMG were dissolved in anhydrous DMF and stirred for 72 h at 50–60 °C under a nitrogen gas atmosphere. After stirring, the reaction mixture was precipitated by adding ether, and the precipitate was repeatedly recovered by centrifugation. The precipitate was dissolved in distilled water, placed in a dialysis tube, and dialyzed sequentially against 0.1 M NaCl solution and then distilled water. The dialyzed product was then lyophilized and stored before use. The synthesized compounds were characterized using Nuclear magnetic resonance (NMR) spectroscopy (Bruker, Billerica, MA).

2.3. Preparation and characterization of HA-LNP

PEG-LNP was synthesized as described elsewhere [31]. Briefly, lipids were dissolved in ethanol at a molar ratio of 50:40:9:1 (SM-102: DSPC: cholesterol: DMG-PEG). A separate solution of mRNA was prepared in sodium acetate buffer solution (pH 4.5). For HA-LNP, lipids were dissolved in ethanol at the same molar ratio (SM-102: DSPC: cholesterol). The dissolved solution was loaded into the cartridge of a NanoAssemblr™ Spark™ Lipid Nanoparticle Formation System (Cytiva, Marlborough, MA) along with a separate solution containing HA-DMG and mRNA dissolved in sodium acetate buffer (pH 4.5), as per the manufacturer's protocol. All prepared LNP solutions were stabilized by exposure to PBS (pH 7.4).

To optimize the HA-LNP formulation, an encapsulation efficiency assay was performed. The morphology of the LNPs was characterized by Titan Krios G4 cryo-transmission electron microscopy (cryo-EM) (Thermo-Fisher Scientific, Waltham, MA). The hydrodynamic diameter and surface charge were determined at room temperature using a Zetasizer Pro dynamic light scattering (DLS) system (Malvern, UK). To measure the mRNA complexation and loading efficiency, PTEN mRNA@HA-LNP and naked PTEN mRNA were run through an agarose gel for 10 min at 100 V. The gel was imaged with Amersham™ Imager 600 (GE Healthcare, Chicago, IL).

2.4. In vitro delivery of LNP complex

B16F10 cells (3×10^5 cells per well) were seeded in confocal dishes with complete medium overnight. EGFP mRNA-Cy5@PEG-LNP and EGFP mRNA-Cy5@HA-LNP complexes were added to the dish with fresh medium. Subsequently, the cells were washed with PBS and stained with DAPI. The stained cells were analyzed with LSM 900 CSLM (Carl Zeiss, Germany). For HA pre-incubation tests, a 100-fold molar excess of HA was added to the well before treatment. EGFP mRNA@PEG-LNP and EGFP mRNA@HA-LNP, EGFP mRNA@Lipofecatmine complexes were added to the plate. After 6 h of incubation, fluorescence was measured using a SPARK 10 M (TECAN, Männedorf, Switzerland). To study the receptor-mediated endocytosis of HA-LNP, the cells were seeded in 6-well plates at a density of 2.5×10^5 cells per well and incubated overnight. For the competitive binding assay, a 100-fold molar excess of HA was added to the well with fresh serum-free medium for 24 h. EGFP mRNA complexes were added to the plate with fresh medium. After 24 h of incubation, the cells were washed twice with PBS and then treated with trypsin for 5 min. They were collected and washed with PBS twice. The cells were analyzed by fluorescence-activated cell sorting (FACS) CytoFlex SRT (Beckman Coulter).

2.5. Cytotoxicity of HA-LNP

B16F10 cells were seeded in 96-well plates at a density of 4×10^4 cells per well with 100 μL of DMEM containing 10 % FBS and 1 % penicillin/streptomycin in 5 % CO_2 incubator at 37 °C. On the following day, the replaced media contained naked PTEN mRNA, PTEN mRNA@PEG-LNP, or PTEN mRNA@HA-LNP complexes at various mRNA concentrations (125, 250, 500, 750, or 1000 ng/mL). The cytotoxicity of LNPs without mRNA was evaluated using the same method. The cytotoxicity assay was performed according to the manufacturer's instructions. Briefly, the assay solution equivalent to 10 % of the media volume was applied. After 2 h of incubation with gentle agitation, absorbance was measured at 450 nm using a Spectramax ABS (Molecular Devices, Sunnyvale, CA) plate reader. Cell viability was calculated using the following equation:

$$\text{Viability } (\%) = \frac{\textit{Sample well absorbance} - \textit{Blank well absorbance}}{\textit{Control well absorbance} - \textit{Blank well absorbance}} \times 100.$$

2.6. Real-time PCR

The culture medium was removed, and the cells were washed with PBS. mRNA was isolated by treating the cells with TRIZOL according to the manufacturer's instructions and centrifugation. cDNA synthesis was conducted using the ReverTra Ace™ qPCR RT Master Mix kit (Osaka, Japan) following the manufacturer's instructions. Quantitative analysis was performed using SYBR Green (Bio-Rad, Hercules, CA) and the CFX Connect Real-Time PCR Detection System (Bio-Rad, Hercules, CA) with the following primers: 5′-TTTGAGAGTTGAGCCGCTGT-3′ and 5′-ATGCTTTGAATCCAAAAACCTTACT-3′. The mRNA levels were normalized against GAPDH.

2.7. Western blot

B16F10 cells were seeded into 6-well plates at a density of 3×10^5 cells per well. After overnight incubation to ensure cell adherence, the culture medium was changed with fresh culture medium containing either PBS, naked PTEN mRNA, PTEN mRNA@PEG-LNP, or PTEN mRNA@HA-LNP. Following a 48 h of incubation, the culture medium was aspirated and all cells were washed with PBS before being treated with the lysis buffer. Total protein concentration was quantified using the BCA assay kit. Fifty μg of each protein sample was loaded into the wells of the SDS-PAGE gel and transferred to the PVDF membrane. The membrane was blocked with 5 % blocking buffer. Primary antibodies for β-actin (1:1000) and PTEN (1 μg/mL) were applied and the membrane was incubated overnight at 4 °C. After washing with TBST thrice, the membrane was incubated with the secondary antibodies according to the manufacturer's manual at room temperature. The membrane was visualized using the Amersham Imager 680 (GE Healthcare, Chicago, IL).

2.8. Immunofluorescence staining

Cells were seeded into confocal plates at a density of 3×10^5 cells per well. After overnight incubation to ensure cell adherence, the culture medium was changed with fresh culture medium containing either PBS, naked PTEN mRNA, PTEN mRNA@PEG-LNP, or PTEN mRNA@HA-LNP. After 48 h of incubation, the culture medium was aspirated, and all cells were washed with PBS before being fixed with 4 % paraformaldehyde. Cells were permeabilized using Triton X-100 solution for 10 min, followed with 5 % bovine serum albumin (BSA) blocking buffer for 1 h. The dishes were incubated overnight at 4 °C with primary antibodies against CRT and PTEN (1:250). After that, the cell nuclei were stained with DAPI and washed again with PBS. Images were captured with Leica Microsystems CMS GmbH and TCapture software was used to acquire the images.

2.9. Detection of cytokines

To assess ATP release from tumor cells, B16F10 cells were seeded in a six-well plate at a density of 4×10^5 cells per well and incubated overnight with 1.5 mL of medium containing 10 % FBS. On the following day, the culture medium was removed from the 6-well plates and replaced with 1.5 mL of fresh medium containing either PBS, naked PTEN mRNA, PTEN mRNA@PEG-LNP, or PTEN mRNA@HA-LNP. The cells were incubated for 48 h, and the supernatants were collected for subsequent analysis. The collected cell culture medium was measured with an ATP assay kit. To evaluate the intertumoral levels of ATP, HMGB-1, and TNF-α, tumor tissues were harvested from experimental animals and homogenized in a tissue extraction solution with protease inhibitors. The supernatants were measured according to the manufacturer's protocols. Cytokine levels in supernatants from tumor tissue homogenates were quantified using the ATP assay kit, the HMGB-1 ELISA kit, and the TNF-α ELISA kit, according to the manufacturers' protocols.

2.10. Animal tests

Six-week-old BALB/c nude mice were used to investigate LNP transdermal delivery, and C57BL/6 mice approximately 6 weeks old were used to investigate immune responses. All mice bred in pathogen-free facilities at Pohang University of Science and Technology (POSTECH) were used in these studies. All mouse experiments were conducted in accordance with a protocol approved by the Institutional Animal Care and Use Committee of POSTECH (2024–0068, 2024–0095).

2.11. In vivo and ex vivo transdermal delivery of Cy5-conjugated mRNA

A subcutaneous melanoma mouse model was established by injecting B16F10 cells (1×10^6 cells/mL) into the left flank. After 7 days, mice were anesthetized, and PBS, EGFP mRNA-Cy5@PEG-LNP, and EGFP mRNA-Cy5@HA-LNP were topically applied to the surface of tumor skin tissue. The mice were kept immobile under anesthesia for 60 min to ensure adequate contact time, followed by a thorough wash with PBS. After bioimaging with *in vivo* imaging system (IVIS) (Revvity, Waltham, MA), mice were sacrificed, their organs were harvested for *ex vivo* analysis, and then sections were cut to a thickness of 5 μm. The transdermal delivery of EGFP mRNA-Cy5@PEG-LNP and EGFP mRNA-Cy5@HA-LNP was assessed by detecting the intensity of Cy5 at 640 nm wavelength with LSM 900 with Airyscan 2 (ZEISS, Germany). Following the same protocol, PBS, naked EGFP mRNA-Cy5, EGFP mRNA-Cy5@PEG-LNP, and EGFP mRNA-Cy5@HA-LNP were topically applied to the surface of porcine skin and incubated at room temperature for 4 h before analysis to assess transdermal delivery.

2.12. In vivo tumor treatment with PTEN mRNA@HA-LNP complex

After 7 days of establishing the subcutaneous melanoma mouse model, when the tumor volume reached approximately 70 mm^3, PBS was used as a control, along with naked PTEN mRNA, PTEN mRNA@PEG-LNP, and PTEN mRNA@HA-LNP, which were topically applied to the tumor site on the skin of the mice. LNPs were topically applied to the tumor skin surface for 60 min while the mice were anesthetized and immobilized. LNP groups received an mRNA dose of 700 μg/kg on days 7, 10, and 13. The tumor size was measured every 2 days, and the average tumor volume was calculated using the formula: (length × width^2)/2. Two days after the final treatment with mRNA complexes, the mice were sacrificed to harvest tumors for cytokine analysis and ICD assessment.

2.13. Histological analysis of tumor apoptosis

After 15 days of *in vivo* treatment, mice were sacrificed for

histological analysis with hematoxylin and eosin (H&E) and TUNEL staining. The tumors were collected and fixed in 4 % formaldehyde. The prepared paraffin slices were visualized and examined with a DMi8 light microscope (Leica, Germany). The TUNEL assay kit was used to detect apoptotic cells according to the manufacturer's instructions. Fluorescence images were captured with Leica Microsystems CMS GmbH, and TCapture software was used to acquire the images.

2.14. Statistical analysis

Statistical analysis was performed using the *t*-test in SigmaPlot 12.5 software (Systat Software Inc., San Jose, CA). The values for $^{*}P < 0.05$, $^{**}P < 0.01$, and $^{***}P < 0.001$ were considered statistically significant. All data are represented as means ± standard deviation (SD) from several separate experiments.

3. Results and discussion

3.1. Characteristics of HA-DMG and HA-LNP

LNPs have emerged as a remarkable delivery platform for mRNA-based therapeutics, as demonstrated by the clinical success of the BioNTech/Pfizer and Moderna COVID-19 vaccines. These vaccines rely on the intramuscular administration of LNPs, which are composed of ionizable lipids, cholesterol, helper lipids, and PEGylated lipids. PEG has long been employed to enhance the stability of therapeutics, including proteins, liposomes, antibodies, and LNPs, by reducing aggregation. However, PEG is associated with notable drawbacks, including hypersensitivity reactions (HSRs) [32–34]. To address these limitations, we developed HA-LNP by replacing PEGylated lipids with HA-conjugated lipids. Our previous work demonstrated that HA improved both transdermal penetration and cell-specific targeting [23]. As a natural ligand for the CD44 receptor, highly expressed on many tumor cells, HA facilitates selective uptake into cancerous tissues. Additionally, the low-molecular-weight HA is known to modulate the tumor microenvironment (TME) and acts as an immunological adjuvant, enhancing anti-tumor immune responses [35,36]. HA-LNP offers a dual advantage: effective transdermal delivery and immunomodulatory potential, making it a promising platform for cancer immunotherapy (Fig. 1).

As illustrated in Fig. 1A, the HA-LNP formulation comprises four main components: an ionizable lipid, a helper lipid, cholesterol, and HA-DMG, a hyaluronate-conjugated lipid. These components were mixed with mRNA using a microfluidic mixing system to ensure uniform particle formation. Unlike conventional PEG-containing LNPs, our formulation integrates HA directly into the lipid bilayer, enhancing CD44-mediated targeting, skin penetration, and immunological engagement within the TME. The incorporation of HA enables transdermal delivery and cancer cell targeting *via* HA receptor-mediated endocytosis (Fig. 1B). HA-LNP facilitates endosomal escape and cytoplasmic release of PTEN mRNA, thereby initiating PTEN expression. This induces ICD, triggers the release of DAMPs, and promotes T cell activation (Fig. 1C).

HA-DMG was designed as an amphiphilic molecule, consisting of a hydrophilic segment derived from HA and a hydrophobic segment from DMG (Fig. 2A). The HA-DMG lipid was synthesized *via* the tosylation reaction (Fig. S1) using low molecular weight HA (5 kDa) to enhance its adjuvant-like effects with a controlled particle size. The synthesis strategy used the single reducing end of the HA polymer chain for conjugation *via* reductive amination with diaminobutane, followed by reaction with tosylated DMG, aiming for site-specific conjugation. The successful synthesis of HA-DMG was confirmed by ^{1}H NMR analysis (Fig. S2A). The degree of substitution was calculated using the integral of the acetyl protons of the HA backbone *versus* the integral of the

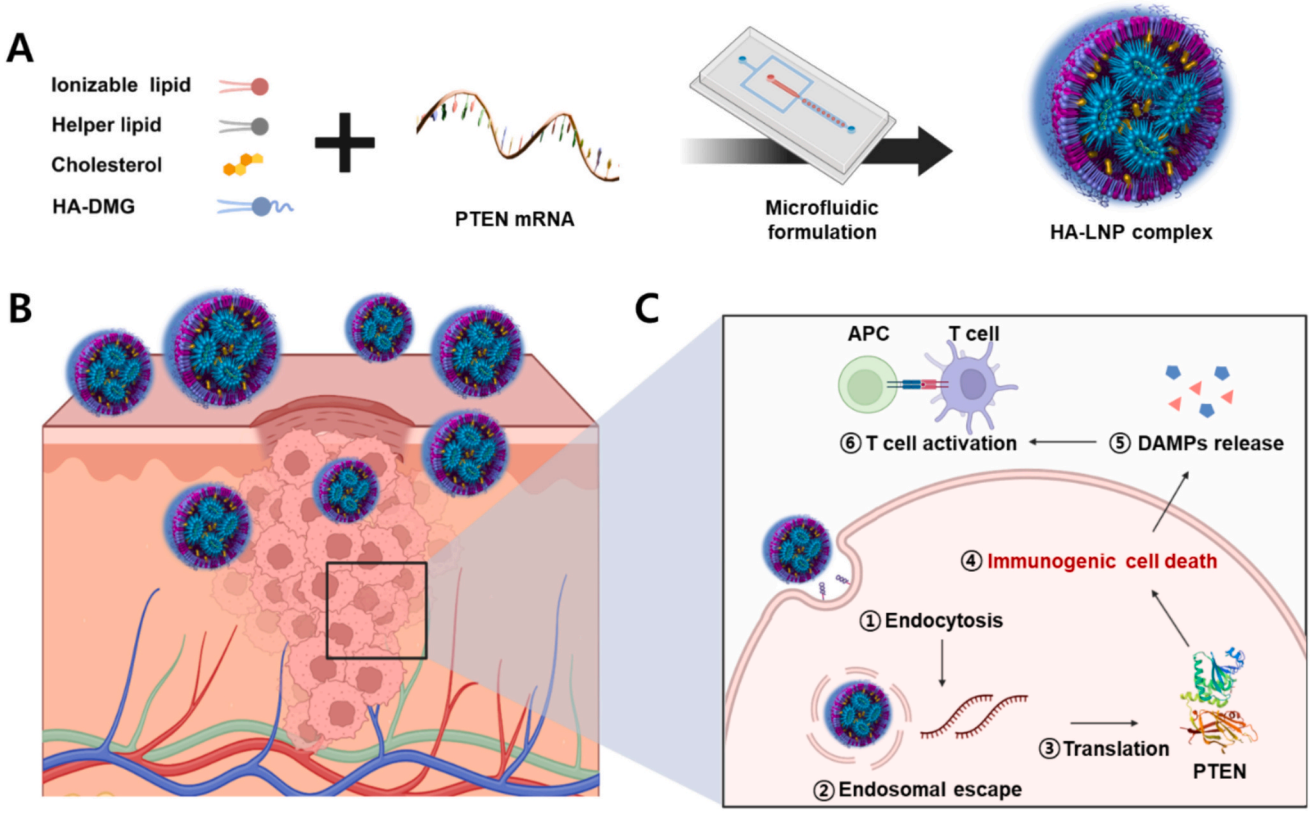

Fig. 1. Schematic illustration for the design and therapeutic strategy of the HA-LNP complex (created with BioRender.com). (A) The HA-LNP, comprising ionizable lipid, helper lipid, cholesterol, and hyaluronated lipid, is formulated with mRNA using a microfluidic system. (B) The incorporation of HA enables transdermal delivery and cancer cell targeting *via* HA receptor-mediated endocytosis. (C) Once internalized, the HA-LNP facilitates the endosomal escape and cytoplasmic release of mRNA, triggering PTEN expression. This induces immunogenic cell death (ICD), enhances the release of DAMPs, and promotes T cell activation.

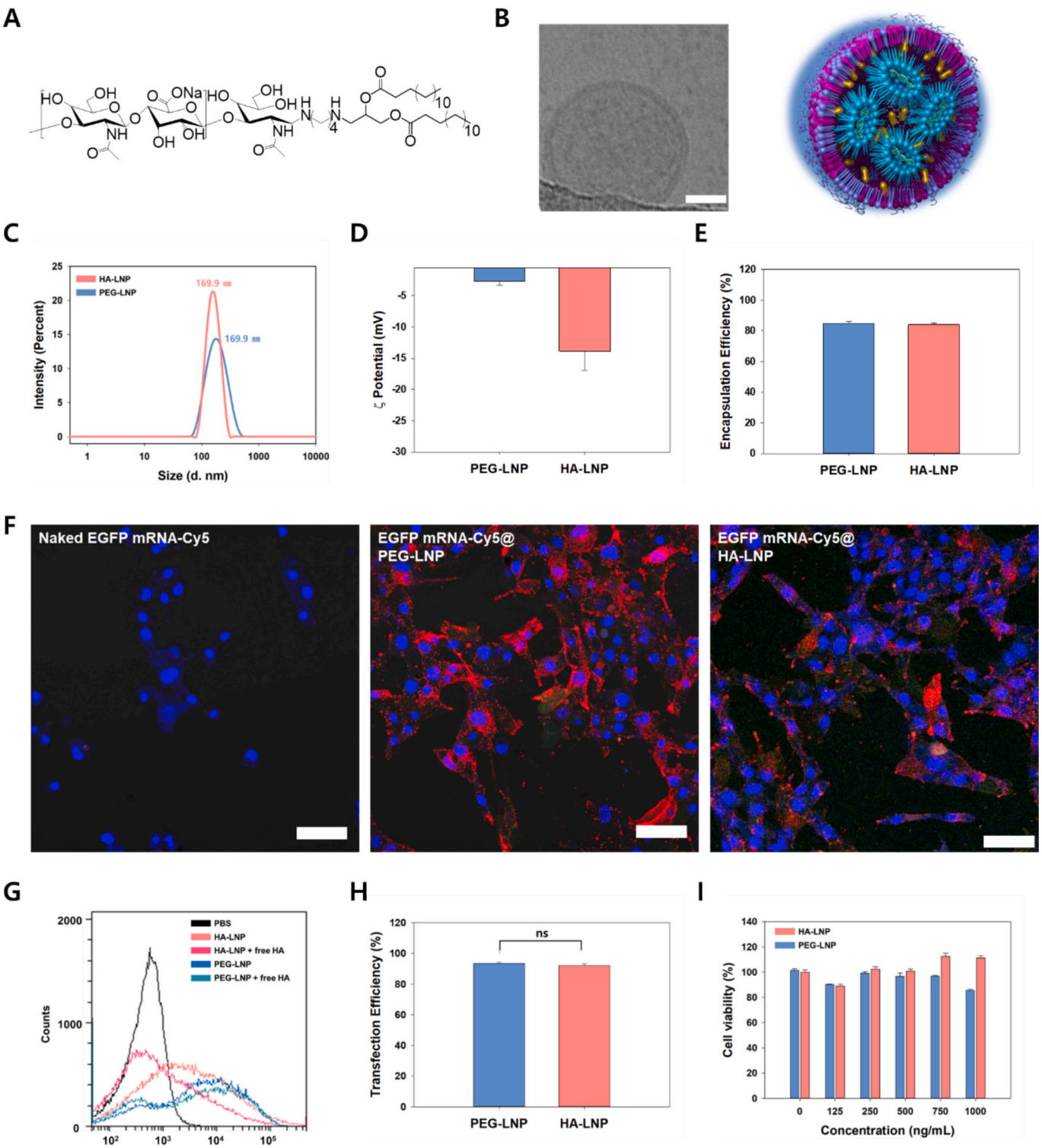

Fig. 2. Synthesis and characterization of EGFP mRNA@HA-LNP complexes. (A) Chemical structure of HA-DMG. (B) Cryo-EM image of HA-LNP (scale bar = 50 nm) alongside a schematic illustration showing HA presentation on the LNP surface. (C) Size distribution, (D) ζ potential, and (E) mRNA encapsulation efficiency of PEG-LNP and HA-LNP complexes. (F) Confocal laser scanning microscopy (CLSM) images of DAPI-stained B16F10 cells showing internalized Cy5-labeled EGFP mRNA delivered *via* different LNP formulations (Scale bars = 50 μm). (G) Flow cytometry graphs of competitive binding assay demonstrating reduced HA-LNP uptake upon HA receptor blocking, confirming CD44-mediated endocytosis ($n = 3$, mean ± SD, two-tailed Student's *t*-test, $^{***}P < 0.001$). (H) Transfection efficiency of PEG-LNP and HA-LNP complexes in B16F10 cells (n = 3, mean ± SD, two-tailed Student's t-test, ns: not significant). (I) Cell viability of B16F10 cells treated with increasing concentrations of EGFP mRNA delivered *via* PEG-LNP or HA-LNP.

terminal methyl protons of the DMG alkyl chains. HA was functionalized with approximately 13.67 ± 0.64 mol% of DMG (Fig. S2B). In addition, gel permeation chromatography (GPC) analysis showed the slight increase in the molecular weight and the peak shift in the retention time for HA-DMG compared with that of the 5 kDa HA backbone (Fig. S3).

The optimal N/P ratio for mRNA complexation was determined using an agarose gel retardation assay (Fig. S4). No mRNA leakage was observed when the N/P ratio exceeded 6, reflecting efficient mRNA encapsulation *via* electrostatic interactions. In accordance, all subsequent HA-LNP formulations were prepared at an N/P ratio of 6. The morphology of the HA-LNP was analyzed by cryogenic electron microscopy (cryo-EM), which revealed spherical nanoparticles with a distinct lipid bilayer structure and a layered surface architecture (Fig. 2B). Dynamic light scattering (DLS) analysis showed a hydrodynamic diameter of 169.9 nm (Fig. 2C). Furthermore, the colloidal stability of HA-LNP was evaluated under physiological conditions. The HA-LNP maintained a stable particle morphology over 24 h, confirming their stability (Fig. S5). Zeta (ζ) potential analysis exhibited that HA-LNP had a surface charge of −13.86 ± 3 mV, significantly more negative than that of PEG-LNP (−2.65 ± 0.6 mV), likely due to the presence of negatively charged HA on the particle surface (Fig. 2D). While ζ potential differences were noted, they are not the primary determinant of transfection efficiency. As reported elsewhere [37,38], factors such as particle size, lipid composition, and surface chemistry have a greater influence. To assess mRNA encapsulation efficiency, Ribogreen™ assays were performed using EGFP mRNA, showing comparable encapsulation efficiencies of 84.04 ± 1.19 % for HA-LNP and 84.87 ± 1.40 % for PEG-LNP (Fig. 2E).

Cellular uptake and gene expression were evaluated in B16F10 melanoma cells using Cy5-labeled EGFP mRNA formulated in PEG-LNP or HA-LNP, or delivered as naked mRNA. Confocal laser scanning microscopy (CLSM) showed efficient cellular uptake and EGFP expression in both PEG-LNP and HA-LNP groups, whereas naked mRNA exhibited neither uptake nor expression (Fig. 2F and S6). To quantitatively confirm the HA receptor-mediated uptake, cells were pretreated with excess free HA to block CD44 receptors prior to LNP exposure. Following HA pretreatment, HA-LNP showed a significant reduction in EGFP expression, whereas the uptake of PEG-LNP was unaffected (Fig. 2G). According to the FACS analysis, the percentage of EGF-positive cells was 54.46 % for HA-LNP, compared to 29.21 % for PEG-LNP. This competitive inhibition provides direct quantitative evidence that HA-LNP uptake occurs primarily *via* HA receptor-mediated endocytosis with specificity.

We further confirmed that HA-LNP facilitated the efficient cytosolic delivery and translation of EGFP mRNA in B16F10 cells with the performance comparable to lipofectamine (Fig. 2H). To evaluate biocompatibility, cytotoxicity assays were performed after 48 h of exposure to various concentrations of EGFP mRNA-loaded PEG-LNP or HA-LNs (Fig. 2I). At concentrations above 750 ng/mL, HA-LNP-treated cells exhibited higher viability than PEG-LNP-treated cells. This may be attributed to the biological activity of HA, which has been reported to support cell proliferation and interactions with the extracellular matrix [39–41]. Collectively, these results demonstrate that HA-DMG can effectively replace PEG in LNP formulations, maintaining nanoparticle uniformity, stability, and transfection efficiency, while also offering enhanced biocompatibility and targeted delivery *via* HA receptor-mediated endocytosis.

3.2. Transdermal penetration of HA-LNP in porcine skin and mouse melanoma models

The transdermal delivery of HA-LNP was first evaluated *ex vivo* in porcine skin. EGFP mRNA-Cy5@HA-LNP was topically applied, and the cross-sections of the treated skin were analyzed by CLSM after 24 h. Strong fluorescence signals, indicative of mRNA localization, were observed deep within the skin layers in the HA-LNP group, reflecting efficient skin penetration, whereas only weak signals were detected in the other groups (Fig. 3A). As this is non-viable tissue, EGFP protein expression was not expected. This enhanced penetration might be attributed to the properties of HA, including its ability to disrupt lipid bilayers, increase skin hydration, and interact with highly expressed CD44 receptors in the skin and the TME. Given the high density of CD44 receptors in tumors, HA-LNP is also expected to exhibit tumor-targeting capability [42]. These findings suggest that HA-LNP offers superior skin permeability and targeted delivery compared to PEG-LNP, supporting their great potential for transdermal mRNA therapy.

To validate these findings *in vivo*, a xenograft melanoma model was established by subcutaneously injecting B16F10 cells into BALB/c nude mice. EGFP mRNA-Cy5@HA-LNP was topically administered to tumor-bearing skin. After 24 h, the skin and tumor tissues were excised, cryosectioned, and examined *via* CLSM. In the PEG-LNP group, Cy5 fluorescence was limited to the skin surface, whereas the HA-LNP group exhibited strong fluorescence throughout the dermis and within tumor tissue (Fig. 3B). Additionally, intracellular EGFP expression within the tumor confirmed the successful delivery and translation of mRNA *in vivo*. IVIS imaging further confirmed the precise localization of HA-LNP within the tumor tissue, with negligible signal detected in major organs such as the spleen, indicating minimal systemic circulation (Fig. S7). These results demonstrate that HA-LNP enables efficient transdermal penetration and tumor-specific delivery, validating its feasibility for non-invasive cancer gene therapy.

3.3. In vitro delivery and ICD induction of PTEN mRNA@HA-LNP

PTEN is a well-established tumor suppressor gene, and its restoration can promote ICD and the release of DAMPs, which initiate immune responses against cancer cells. To assess the effect of PTEN restoration on tumor cell viability, B16F10 cells were treated with PBS, naked PTEN mRNA, PTEN mRNA@PEG-LNP, or PTEN mRNA@HA-LNP at varying mRNA concentrations (Fig. 4A). Cell viability was assessed 48 h post-treatment and normalized to the PBS-treated control. Both PTEN mRNA@PEG-LNP and PTEN mRNA@HA-LNP induced the dose-dependent cytotoxicity. The half-maximal inhibitory concentration (IC_{50}) was approximately 500 ng/mL for both PEG- and HA-LNP formulations. In contrast, naked PTEN mRNA did not produce a significant reduction in cell viability at any tested concentration.

To investigate whether PTEN-induced cell death was immunogenic, we measured two hallmark DAMPs: cell-surface exposure of calreticulin (CRT) and extracellular ATP release. CRT is an endoplasmic reticulum chaperone and translocates to the cell surface during ICD and serves as an “eat-me” signal that promotes phagocytosis and antigen presentation by dendritic cells. ATP is released into the extracellular space during ICD and acts as a chemoattractant, recruiting and activating immune cells, particularly dendritic cells. Together, CRT exposure and ATP release enable the robust assessment of ICD and its potential to stimulate an antitumor immune response. CRT surface expression was evaluated *via* immunofluorescence staining and CLSM. CRT exposure was observed in the PTEN mRNA@PEG-LNP, and PTEN mRNA@HA-LNP groups after 48 h, with the HA-LNP group displaying the highest levels of CRT expression (Fig. 4B). This result suggests that the low molecular weight of HA (LMW-HA) may have promoted the CRT expression by increasing endoplasmic reticulum (ER) stress [43]. ATP release was quantified by ATP assay, and both PEG-LNP and HA-LNP resulted in significantly elevated ATP secretion compared to the control (Fig. 4C). Quantitative analysis of fluorescence intensity confirmed that HA-LNP results in markedly higher CRT exposure than PEG-LNP (Fig. 4D).

The enhanced ICD observed with HA-LNP, despite comparable transfection efficiencies with PEG-LNP (Fig. 2H), suggests a synergistic effect between PTEN restoration and the properties of HA carrier itself. This mechanism likely involves two cooperative immunogenic interactions. First, the restoration of PTEN expression induces endoplasmic reticulum (ER) stress, a well-established trigger of CRT translocation to the cell surface [15]. This is the primary ICD-inducing

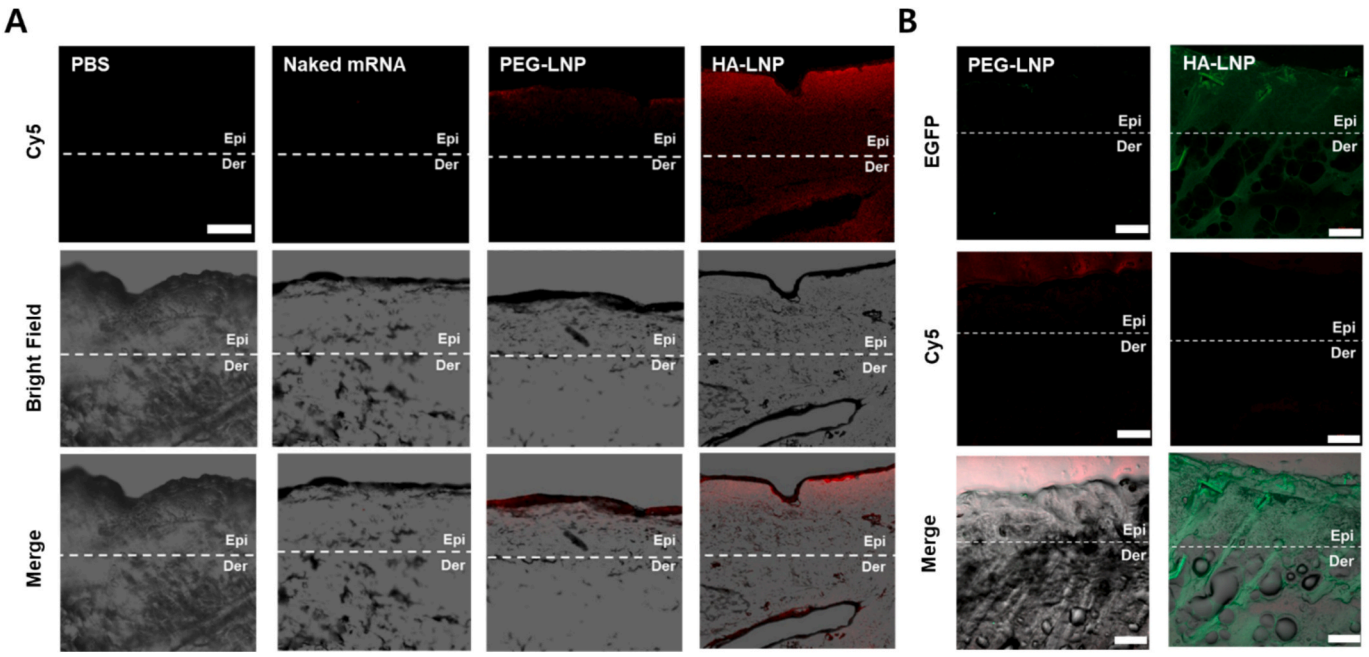

Fig. 3. Transdermal penetration of HA-LNP in porcine skin and mouse melanoma models (Epi: Epidermis, Der: Dermis). (A) CLSM images of porcine skin following 24 h topical application of EGFP mRNA-Cy5 formulated with PEG-LNP or HA-LNP (scale bars = 100 μm). (B) CLSM images of skin and tumor tissues from B16F10 tumor-bearing mice after topical application of naked EGFP mRNA-Cy5, EGFP mRNA-Cy5@PEG-LNP, or EGFP mRNA-Cy5@HA-LNP (scale bars = 100 μm).

mechanism shared by both formulations. Second, the 5 kDa HA used in the HA-DMG conjugate serves as a DAMP signal recognized as a pro-inflammatory, immunostimulatory molecule [43]. The LMW-HA can activate immune cells *via* toll-like receptor (TLR) 2, TLR 4, and CD44 signaling. Thus, HA-LNP delivers two distinct immunogenic signals: (1) DAMP signals released by the PTEN-induced cell death and (2) the intrinsic DAMP-like activity of LMW-HA. This dual stimulation creates a more potent pro-ICD environment, leading to the observed increase in the CRT exposure [44]

RT-PCR, immunofluorescence, and western blot analyses were conducted to confirm the intracellular delivery of PTEN mRNA and subsequent protein expression mediated by the LNP. RT-PCR analysis confirmed significantly elevated PTEN mRNA levels in cells treated with both LNP formulations (Fig. 4E). Immunofluorescence staining confirmed the cytoplasmic accumulation of the PTEN protein (Fig. 4F). Western blot analysis further validated the successful restoration of PTEN protein expression following treatment with the LNP formulations (Fig. 4G).

3.4. The antitumor effect of PTEN mRNA@HA-LNP in B16F10 tumor-bearing mouse models

Based on *in vitro* findings, we evaluated the therapeutic efficacy and immunostimulatory effect of PTEN mRNA@HA-LNP *in vivo* using a B16F10 melanoma mouse model. To establish the model, 4×10^5 B16F10 cells were subcutaneously injected into the right flank of C57BL/6 mice (Fig. 5A). When tumors reached an average volume of 60 mm^3 on day 7, the tumor site was treated by topical administration with PBS, naked PTEN mRNA, PTEN mRNA@PEG-LNP, or PTEN mRNA@HA-LNP at a dose of 0.7 μg mRNA per mg body weight. Treatments were repeated on days 7, 10, and 13. The mice were euthanized, and tumor tissues and blood samples were collected on day 14. Macroscopic tumor images and measurements revealed that PTEN mRNA@HA-LNP significantly suppressed tumor growth compared to all other groups (Fig. 5B). Tumor volume and weight were substantially reduced in the HA-LNP group, while the body weight remained stable (Fig. 5C, D, and E), demonstrating its strong antitumor efficacy. Furthermore, histological analysis of normal skin tissue adjacent to the tumor showed no evidence of apoptosis in fibroblasts or normal tissue upon delivery of PTEN mRNA (Fig. S9), supporting the selectivity and safety of this approach.

To assess ICD induction *in vivo*, immunofluorescence staining was performed on tumor sections to assess CRT surface exposure. CRT expression was significantly elevated in the PTEN mRNA@HA-LNP group compared to the other treatments (Fig. 5F), indicating enhanced ICD. ATP release, another hallmark of ICD, was also increased in the HA-LNP group (Fig. 5G), supporting its role in promoting ICD. To further investigate immune activation, we measured HMGB1 levels in serum by ELISA. The PTEN mRNA@HA-LNP group exhibited significantly higher HMGB1 release compared to all other groups, consistent with increased DAMP signaling (Fig. 5H). Additionally, TNF-α levels were quantified to evaluate inflammatory cytokine responses. Significantly elevated TNF-α levels were observed in the HA-LNP group (Fig. 5I), suggesting that modulation of the TME activated the immune system. These results indicate that PTEN mRNA@HA-LNP not only delivers mRNA effectively *via* the transdermal route but also induces robust ICD and stimulates antitumor immune responses, highlighting its feasibility as a non-invasive immunotherapeutic strategy.

3.5. Histological analysis of tumor cell apoptosis

Histological analysis with H&E staining of skin tumor sections revealed minimal morphological alterations in the PBS, naked PTEN mRNA, and PTEN mRNA@PEG-LNP groups, indicating limited therapeutic efficacy (Fig. 6). In contrast, the PTEN mRNA@HA-LNP group exhibited substantial tissue disruption and architectural damage, reflecting effective tumor suppression. The other treatment groups frequently showed features such as chromatin condensation and nuclear irregularities, consistent with aggressive tumor progression. Notably, the PTEN mRNA@HA-LNP group also showed marked macrophage infiltration in tumor tissue (Fig. S8), confirming that the HA-LNP formulation stimulated an immune response and contributed to tumor immunomodulation.

To further assess apoptosis, a TUNEL assay was performed to detect DNA fragmentation, a hallmark of apoptotic cell death caused by

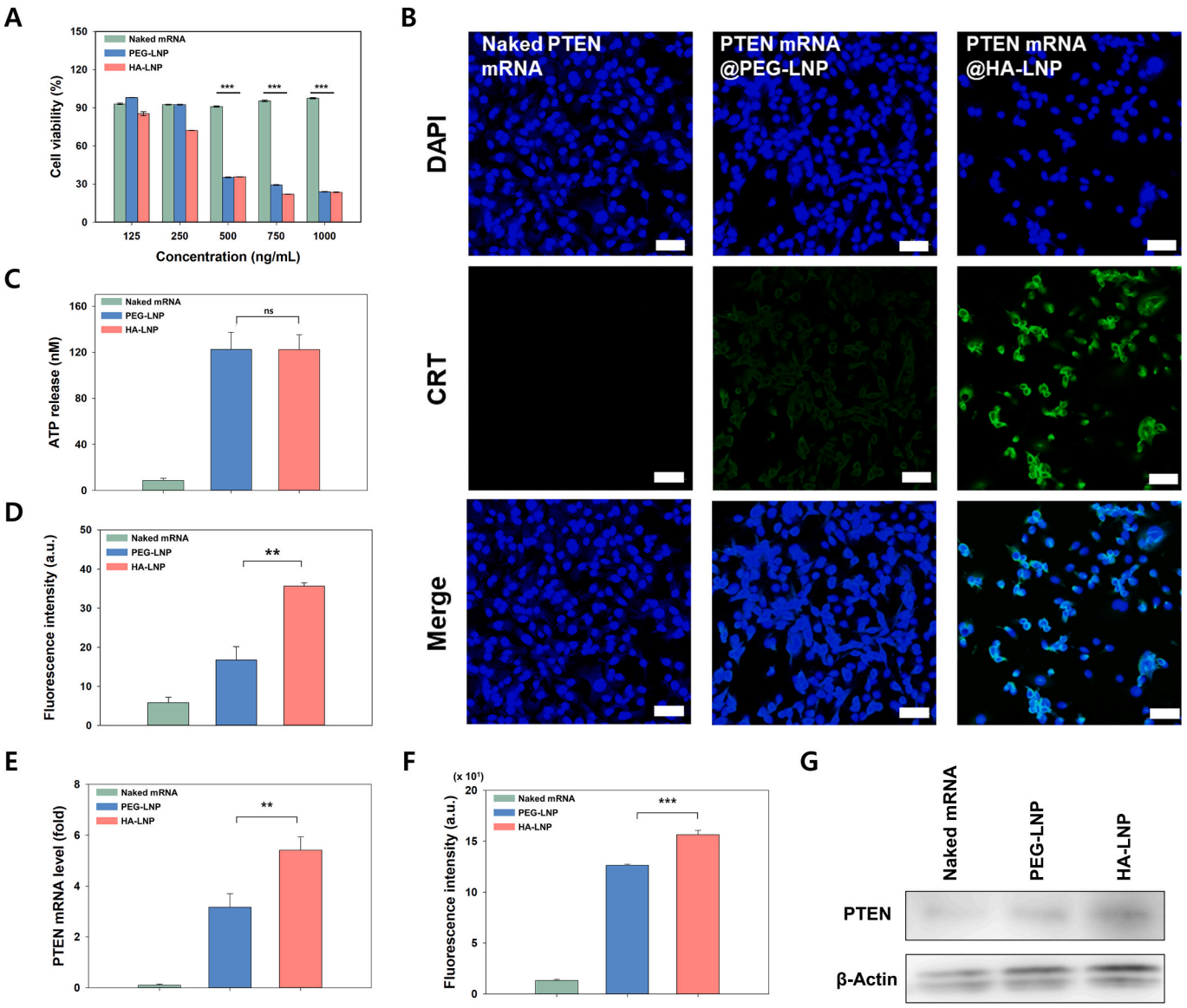

Fig. 4. *In vitro* delivery of PTEN mRNA and induction of ICD in cancer cells. (A) Cell viability of B16F10 cells treated with naked PTEN mRNA, PTEN mRNA@PEG-LNP, and PTEN mRNA@HA-LNP at various mRNA concentrations. Viability is normalized to the PBS-treated control group ($n = 3$, mean ± SD, two-tailed Student's *t*-test, $^{***}P < 0.001$). (B) Surface exposure of CRT assessed by CLSM 48 h after treatment with the indicated PTEN mRNA formulations (scale bar = 50 μm). (C) Quantification of extracellular ATP release using an ATP assay following 48 h treatment with naked PTEN mRNA, PEG-LNP, or HA-LNP formulations (n = 3, mean ± SD, two-tailed Student's t-test). (D) Quantification of CRT Immunofluorescence (n = 3, $^{**}P < 0.01$) (E) The mRNA levels in B16F10 cells were analyzed using RT-PCR (n = 3, mean ± SD, two-tailed Student's t-test, $^{**}P < 0.01$). (F) Quantification of PTEN Immunofluorescence (n = 3, $^{**}P < 0.01$) (G) Western blot analysis of PTEN expression after 48 h treatment.

endonuclease-mediated DNA cleavage. The PTEN mRNA@HA-LNP group exhibited significantly stronger TUNEL-positive signals than the other groups (Fig. 6), indicating enhanced apoptosis. These histological findings confirm that HA-LNP enables efficient transdermal delivery of PTEN mRNA to tumor tissues, leading to effective induction of tumor cell apoptosis and modulation of the TME.

4. Conclusions

We achieved non-invasive transdermal mRNA delivery by incorporating HA-DMG directly into the LNP formulation to encapsulate full-length PTEN mRNA for cancer immunotherapy. The HA-DMG played a multifunctional role in the formulation: replacing PEG to maintain nanoparticle stability and biocompatibility, enabling transdermal penetration, and mediating specific targeting to CD44-expressing cells in the TME. Furthermore, the use of LMW-HA appears to synergize with PTEN restoration to enhance ICD induction, likely through its intrinsic activity as a DAMP signal. This dual functionality distinguishes HA-LNP from conventional PEG-based LNP, highlighting their potential as a versatile, non-invasive delivery system. Overall, our transdermal HA-LNP platform offers a promising approach for mRNA-based cancer immunotherapy, particularly in tumors harboring PTEN loss-of-function mutations. The topical application strategy is particularly relevant for accessible tumors such as melanoma, offering high patient compliance and localized delivery with minimal systemic exposure. In addition to its therapeutic efficacy, the system exhibits remarkable safety, biocompatibility, and manufacturing scalability, facilitating its clinical translation. While the current study demonstrates significant local tumor control, it did not evaluate the efficacy against metastatic tumors or the ability to prevent relapse. Future studies will focus on assessing the long-

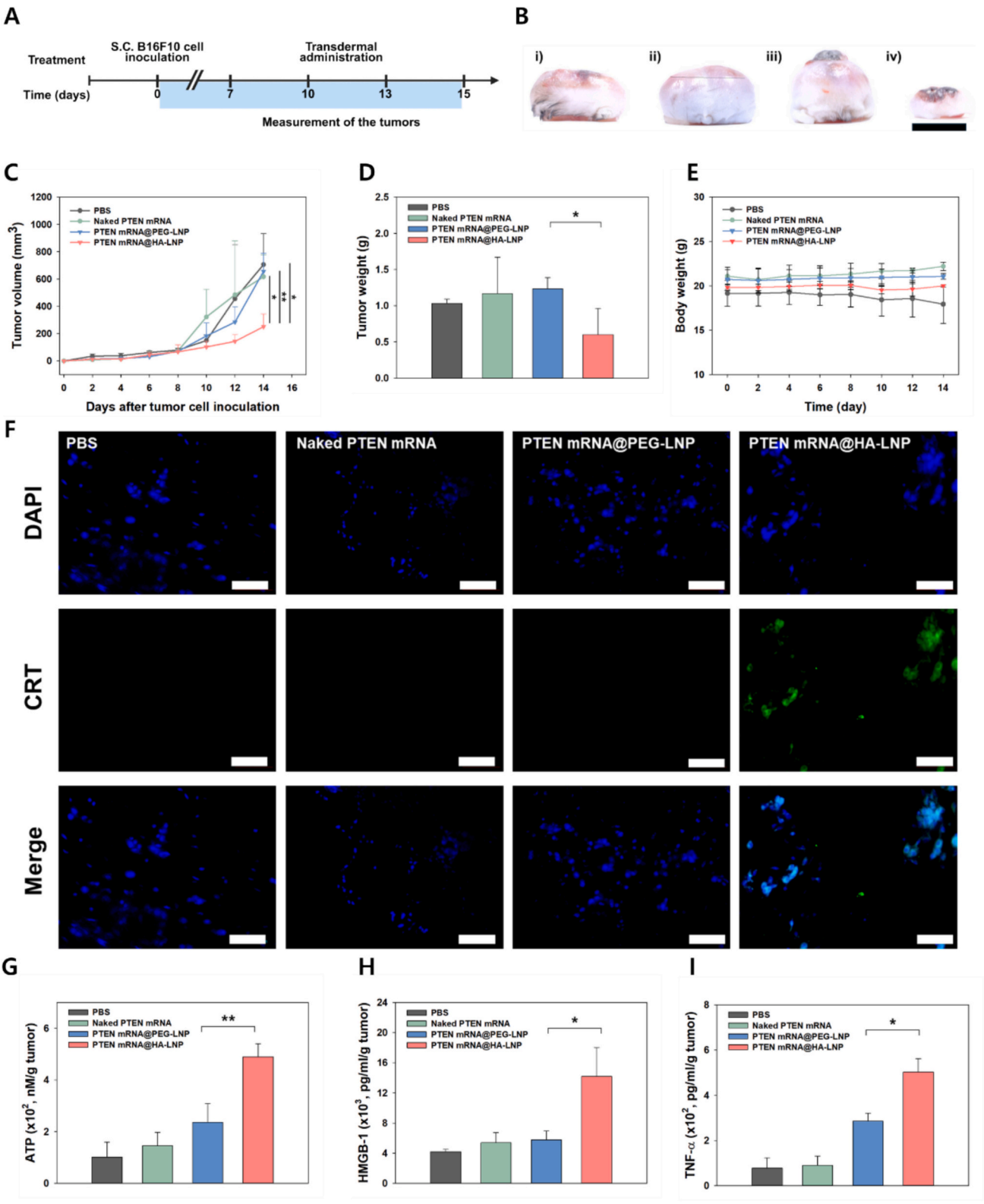

Fig. 5. The antitumor effect of PTEN mRNA@HA-LNP in a B16F10 tumor-bearing mouse model. (A) Schematic timeline of the therapeutic regimen in the B16F10 melanoma model. (B) Representative images of excised tumors from mice treated with (i) PBS, (ii) naked PTEN mRNA, (iii) PTEN mRNA@PEG-LNP, or (iv) PTEN mRNA@HA-LNP (scale bar = 10 mm). (C) Tumor growth curves showing the average tumor size over time ($n = 3$, mean ± SD, two-tailed Student's t-test, $^{*}P < 0.05$, $^{**}P < 0.01$). (D) Final tumor weights at the endpoint (14 days) ($n = 3$, mean ± SD, two-tailed Student's t-test, $^{*}P < 0.05$). (E) Body weight. (F) Immunofluorescence staining of CRT in tumor tissues post-treatment (scale bar = 100 μm). (G) Quantification of extracellular ATP levels in tumor supernatants by the ATP metabolism assay ($n = 3$, mean ± SD, two-tailed Student's t-test, $^{**}P < 0.01$). (H) HMGB1 expression in tumor lysates measured by ELISA ($n = 3$, mean ± SD, two-tailed Student's t-test, $^{*}P < 0.05$). (I) TNF-α levels in tumor supernatants determined by ELISA ($n = 3$, mean ± SD, two-tailed Student's t-test, $^{*}P < 0.05$).

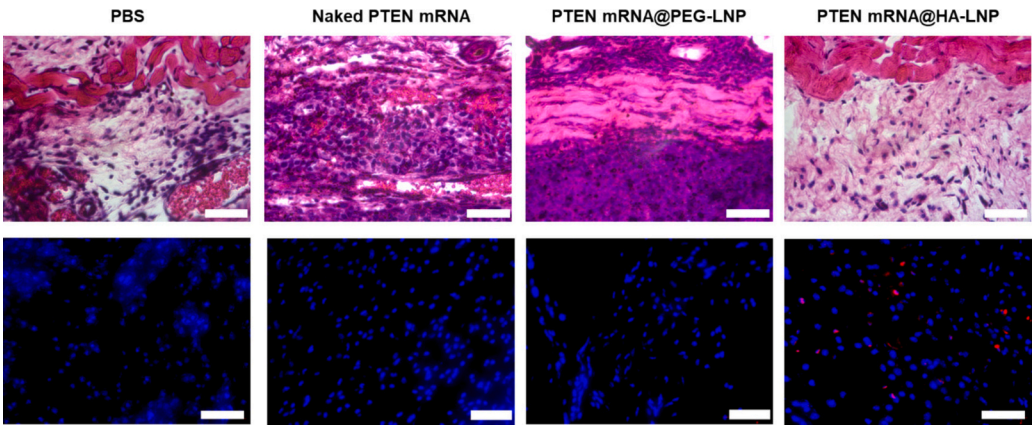

Fig. 6. Histological analysis of tumor cell apoptosis following PTEN mRNA treatment. H&E and TUNEL staining of tumor tissues after treatment with PBS, naked PTEN mRNA, PTEN mRNA@PEG-LNP, or PTEN mRNA@HA-LNP (scale bar = 100 μm).

term immunological memory effect of this treatment, including its effectiveness in avoiding tumor relapses and controlling metastatic cancer, and further validating the versatility of HA-LNP as a next-generation, non-invasive mRNA delivery system.

CRediT authorship contribution statement

Mungu Kim: Writing – review & editing, Writing – original draft, Visualization, Validation, Methodology, Investigation, Formal analysis, Data curation. **Zhengyu Piao:** Writing – review & editing, Methodology, Investigation. **Jin Huh:** Writing – review & editing, Visualization, Supervision. **Sei Kwang Hahn:** Writing – review & editing, Supervision, Project administration, Funding acquisition, Conceptualization.

Acknowledgment

This research was supported by the National Research Foundation (NRF) of Korea (BRIDGE Research Program (RS-2022-NR067643), and Basic Science Research Program, (RS-2025-16072440) of the funded by the Ministry of Science and ICT, Korea. This research was also supported by the Korea Medical Device Development Fund grant (RS-2023-00253749) and the NRF B-IRC grant (RS-2023-00260454) funded by the Korean government. We thank Won Ho Kong (Pohang Techno Park), Daham Jeong (PHI Biomed), and Su Jeong Kim (Institute of Membrane Proteins) for the discussions on LNP and experimental instruments.

Appendix A. Supplementary data

Supplementary data to this article can be found online at https://doi.org/10.1016/j.jconrel.2025.114518.

Data availability

Data will be made available on request.

References

[1] G.V. Long, S.M. Swetter, A.M. Menzies, J.E. Gershenwald, R.A. Scolyer, Cutaneous melanoma, Lancet 402 (2023) 485–502.
[2] J. Berk-Krauss, J.A. Stein, J. Weber, D. Polsky, A.C. Geller, New systematic therapies and trends in cutaneous melanoma deaths among US whites, 1986–2016, Am. J. Public Health 110 (2020) 731–733.
[3] R.S. Moubarak, A. de Pablos-Aragoneses, V. Ortiz-Barahona, Y. Gong, M. Gowen, I. Dolgalev, S.A.A. Shadaloey, D. Argibay, A. Karz, R. Von Itter, E.C. Vega-Sáenz de Miera, E. Sokolova, F. Darvishian, A. Tsirigos, I. Osman, E. Hernando, The histone demethylase PHF8 regulates TGFβ signaling and promotes melanoma metastasis, Sci. Adv. 8 (2022) eabi7127.
[4] M.S. Carlino, J. Larkin, G.V. Long, Immune checkpoint inhibitors in melanoma, Lancet 398 (2021) 1002–1014.
[5] J.X. Lim, T. McTaggart, S.K. Jung, K.J. Smith, G. Hulme, S. Laba, Y.Q. Ng, A. Williams, R. Hussain, J. Coxhead, I. Cosgarea, C. Arden, J. Nsengimana, P. Lovat, G. Anderson, H.-W. Sun, A. Laurence, S. Amarnath, PD-1 receptor deficiency enhances CD30+ Treg cell function in melanoma, Nat. Immunol. 26 (2025) 1074–1086.
[6] A. Kolb, A.-M. Kulis-Mandic, M. Klein, A. Stastny, M. Haist, V. Votteler, B. Weidenthaler-Barth, T. Sinnberg, A. Sucker, G. Allies, L.J. Albrecht, A. Tasdogan, A. Tuettenberg, M.M. Gaida, C. Deppermann, H. Stege, D. Schadendorf, S. Grabbe, K. Schulze-Osthoff, D. Kramer, Constitutive expression of the transcriptional co-activator IκBζ promotes melanoma growth and immunotherapy resistance, Nat. Commun. 16 (2025) 5387.
[7] M. Redrado, M. Houry, K. Hastings, M. Molero-Abraham, T. Lozano, J.L. Solorzano, J. Sanz-Ortega, V. Adradas, R. Amat, E. Redin, S. Leon, N. Legarra, J. Garcia, D. Serrano, K. Valencia, C. Robles-Oteiza, G. Foggetti, N. Otegui, E. Felip, J. J. Lasarte, L. Paz-Ares, J. Zugazagoitia, K. Politi, L. Montuenga, A. Calvo, PTEN loss confers resistance to anti–PD-1 therapy in non–small cell lung cancer by increasing tumor infiltration of regulatory T cells, Cancer Res. 83 (2023) 2513–2526.
[8] H. Kinoh, S. Quader, H. Shibasaki, X. Liu, A. Maity, T. Yamasoba, H. Cabral, K. Kataoka, Translational nanomedicine boosts anti-PD1 therapy to eradicate orthotopic PTEN-negative glioblastoma, ACS Nano 14 (2020) 10127–10140.
[9] J.A. Benitez, J. Ma, M. D'Antonio, A. Boyer, M.F. Camargo, C. Zanca, S. Kelly, A. Khodadadi-Jamayran, N.M. Jameson, M. Andersen, H. Miletic, S. Saberi, K. A. Frazer, W.K. Cavenee, F.B. Furnari, PTEN regulates glioblastoma oncogenesis through chromatin-associated complexes of DAXX and histone H3.3, Nat. Commun. 8 (2017) 15223.
[10] Z.O. Doha, X. Wang, N.L. Calistri, J. Eng, C.J. Daniel, L. Ternes, E.N. Kim, C. Pelz, M. Munks, C. Betts, S. Kwon, E. Bucher, X. Li, T. Waugh, Z. Tatarova, D. Blumberg, A. Ko, N. Kirchberger, J.A. Pietenpol, M.E. Sanders, E.M. Langer, M.-S. Dai, G. Mills, K. Chin, Y.H. Chang, L.M. Coussens, J.W. Gray, L.M. Heiser, R.C. Sears, MYC deregulation and PTEN loss model tumor and stromal heterogeneity of aggressive triple-negative breast cancer, Nat. Commun. 14 (2023) 5665.
[11] T. Jamaspishvili, D.M. Berman, A.E. Ross, H.I. Scher, A.M. De Marzo, J.A. Squire, T.L. Lotan, Clinical implications of PTEN loss in prostate cancer, Nat. Rev. Urol. 15 (2018) 222–234.
[12] K.H.T. Paraiso, Y. Xiang, V.W. Rebecca, E.V. Abel, Y.A. Chen, A.C. Munko, E. Wood, I.V. Fedorenko, V.K. Sondak, A.R.A. Anderson, A. Ribas, M.D. Palma, K. L. Nathanson, J.M. Koomen, J.L. Messina, K.S.M. Smalley, PTEN loss confers BRAF inhibitor resistance to melanoma cells through the suppression of BIM expression, Cancer Res. 71 (2011) 2750–2760.
[13] S. Ramaswamy, N. Nakamura, F. Vazquez, D.B. Batt, S. Perera, T.M. Roberts, W. R. Sellers, Regulation of G1 progression by the PTEN tumor suppressor protein is linked to inhibition of the phosphatidylinositol 3-kinase/Akt pathway, Proc. Natl. Acad. Sci. 96 (1999) 2110–2115.
[14] K. Tumaneng, K. Schlegelmilch, R.C. Russell, D. Yimlamai, H. Basnet, N. Mahadevan, J. Fitamant, N. Bardeesy, F.D. Camargo, K.-L. Guan, YAP mediates crosstalk between the hippo and PI(3)K–TOR pathways by suppressing PTEN via miR-29, Nat. Cell Biol. 14 (2012) 1322–1329.
[15] Y.-R. Lee, M. Chen, P.P. Pandolfi, The functions and regulation of the PTEN tumour suppressor: new modes and prospects, Nat. Rev. Mol. Cell Biol. 19 (2018) 547–562.
[16] J. van Haasteren, J. Li, O.J. Scheideler, N. Murthy, D.V. Schaffer, The delivery challenge: fulfilling the promise of therapeutic genome editing, Nat. Biotechnol. 38 (2020) 845–855.
[17] S. Chen, Q. Chen, X. You, Z. Zhou, N. Kong, F. Ambrosio, Y. Cao, R. Abdi, W. Tao, Using RNA therapeutics to promote healthy aging, Nat. Aging 5 (2025) 968–983.
[18] Y. Lee, M. Jeong, G. Lee, J. Park, H. Jung, S. Im, H. Lee, Development of lipid nanoparticle formulation for the repeated administration of mRNA therapeutics, Biomater. Res 28 (2024) 17.
[19] S. Chen, X. Huang, Y. Xue, E. Álvarez-Benedicto, Y. Shi, W. Chen, S. Koo, D. J. Siegwart, Y. Dong, W. Tao, Nanotechnology-based mRNA vaccines, Nat. Rev. Methods Primers 3 (2023) 63.

[20] H. Chen, D. Liu, J. Guo, A. Aditham, Y. Zhou, J. Tian, S. Luo, J. Ren, A. Hsu, J. Huang, F. Kostas, M. Wu, D.R. Liu, X. Wang, Branched chemically modified poly (a) tails enhance the translation capacity of mRNA, Nat. Biotechnol. 43 (2025) 194–203.
[21] N. Pardi, S. Tuyishime, H. Muramatsu, K. Kariko, B.L. Mui, Y.K. Tam, T.D. Madden, M.J. Hope, D. Weissman, Expression kinetics of nucleoside-modified mRNA delivered in lipid nanoparticles to mice by various routes, J. Control. Release 217 (2015) 345–351.
[22] W.H. Kong, K. Park, M.-Y. Lee, H. Lee, D.K. Sung, S.K. Hahn, Cationic solid lipid nanoparticles derived from apolipoprotein-free LDLs for target specific systemic treatment of liver fibrosis, Biomaterials 34 (2013) 542–551.
[23] Z. Piao, M. Kim, J. Huh, S.K. Hahn, Transdermal hyaluronate/cationic solid lipid nanoparticle/siRNA complex for the treatment of skin cancer, J. Control. Release 385 (2025) 113967.
[24] E.J. Oh, K. Park, K.S. Kim, J. Kim, J.-A. Yang, J.-H. Kong, M.Y. Lee, A.S. Hoffman, S.K. Hahn, Target specific and long-acting delivery of protein, peptide, and nucleotide therapeutics using hyaluronic acid derivatives, J. Control. Release 141 (2010) 2–12.
[25] H. Kim, M. Shin, S. Han, W. Kwon, S.K. Hahn, Hyaluronic acid derivatives for translational medicines, Biomacromolecules 20 (2019) 2889–2903.
[26] H. Kim, H. Jeong, S. Han, S. Beack, B.W. Hwang, M. Shin, S.S. Oh, S.K. Hahn, Hyaluronate and its derivatives for customized biomedical applications, Biomaterials 123 (2017) 155–171.
[27] J. Wang, D. Liu, S. Guan, W. Zhu, L. Fan, Q. Zhang, D. Cai, Hyaluronic acid-modified liposomal honokiol nanocarrier: enhance anti-metastasis and antitumor efficacy against breast cancer, Carbohydr. Polym. 235 (2020) 115981.
[28] S. Mizrahy, S.R. Raz, M. Hasgaard, H. Liu, N. Soffer-Tsur, K. Cohen, R. Dvash, D. Landsman-Milo, M.G.E.G. Bremer, S.M. Moghimi, D. Peer, Hyaluronan-coated nanoparticles: the influence of the molecular weight on CD44-hyaluronan interactions and on the immune response, J. Control. Release 156 (2011) 231–238.
[29] D. Bitounis, E. Jacquinet, M.A. Rogers, M.M. Amiji, Strategies to reduce the risks of mRNA drug and vaccine toxicity, Nat. Rev. Drug Discov. 23 (2024) 281–300.
[30] K.S. Kim, H. Kim, Y. Park, W.H. Kong, S.W. Lee, S.J.J. Kwok, S.K. Hahn, S.H. Yun, Noninvasive transdermal vaccination using hyaluronan nanocarriers and laser adjuvant, Adv. Funct. Mater. 26 (2016) 2512–2522.
[31] M. Pine, G. Arora, T.M. Hart, E. Bettini, B.T. Gaudette, H. Muramatsu, I. Tombácz, T. Kambayashi, Y.K. Tam, D. Brisson, D. Allman, M. Locci, D. Weissman, E. Fikrig, N. Pardi, Development of an mRNA-lipid nanoparticle vaccine against Lyme disease, Mol. Ther. 31 (2023) 2702–2714.
[32] G.T. Kozma, T. Mészáros, I. Vashegyi, T. Fülöp, E. Örfi, L. Dézsi, L. Rosivall, Y. Bavli, R. Urbanics, T.E. Mollnes, Y. Barenholz, J. Szebeni, Pseudo-anaphylaxis to polyethylene glycol (PEG)-coated liposomes: roles of anti-PEG IgM and complement activation in a porcine model of human infusion reactions, ACS Nano 13 (2019) 9315–9324.
[33] M.L. Caballero, M.S. Krantz, S. Quirce, E.J. Phillips, C.A. Stone, Hidden dangers: recognizing excipients as potential causes of drug and vaccine hypersensitivity reactions, J Allergy Clin Immunol Pract 9 (2021) 2968–2982.
[34] Z.-H. Zhou, C.A. Stone, B. Jakubovic, E.J. Phillips, G. Sussman, J. Park, U. Hoang, S.L. Kirshner, R. Levin, S. Kozlowski, Anti-PEG IgE in anaphylaxis associated with polyethylene glycol, J Allergy Clin Immunol Pract 9 (2021) 1731–1733.
[35] A. Dalla Pietà, D. Carpanese, A. Grigoletto, A. Tosi, S. Dalla Santa, G.K. Pedersen, D. Christensen, L. Meléndez-Alafort, V. Barbieri, P. De Benedictis, G. Pasut, I. M. Montagner, A. Rosato, Hyaluronan is a natural and effective immunological adjuvant for protein-based vaccines, Cell. Mol. Immunol. 18 (2021) 1197–1210.
[36] A. Dalla Pietà, B. Genova, A. Penna, A. Sinigaglia, S. Vogiatzis, L. Barzon, M. Pagliari, F. Bonfante, F. Torrigiani, T. Sofia, R. Verin, A. Tosi, D. Carpanese, R. Sommaggio, V. Barbieri, S. Dalla Santa, G. Zuccolotto, A. Grigoletto, G. Pasut, A. Rosato, On the adjuvanticity of hyaluronan: the case of a SARS-CoV-2 vaccine, J. Control. Release 382 (2025) 113674.
[37] Y. Yang, X. Zhang, S. Wu, R. Zhang, B. Zhou, X. Zhang, L. Tang, Y. Tian, K. Men, L. Yang, Enhanced nose-to-brain delivery of siRNA using hyaluronan-enveloped nanomicelles for glioma therapy, J. Control. Release 342 (2022) 66–80.
[38] Y. Zhu, R. Shen, I. Vuong, R.A. Reynolds, M.J. Shears, Z.-C. Yao, Y. Hu, W.J. Cho, J. Kong, S.K. Reddy, S.C. Murphy, H.-Q. Mao, Multi-step screening of DNA/lipid nanoparticles and co-delivery with siRNA to enhance and prolong gene expression, Nat. Commun. 13 (2022) 4282.
[39] M.P. Stewart, A. Sharei, X. Ding, G. Sahay, R. Langer, K.F. Jensen, In vitro and ex vivo strategies for intracellular delivery, Nature 538 (2016) 183–192.
[40] S. Amorim, C.A. Reis, R.L. Reis, R.A. Pires, Extracellular matrix mimics using hyaluronan-based biomaterials, Trends Biotechnol. 39 (2021) 90–104.
[41] T. Yan, X. Chen, H. Zhan, P. Yao, N. Wang, H. Yang, C. Zhang, K. Wang, H. Hu, J. Li, J. Sun, Y. Dong, E. Lu, Z. Zheng, R. Zhang, X. Wang, J. Ma, M. Gao, J. Ye, X. Wang, L. Teng, H. Liu, S. Zhao, Interfering with hyaluronic acid metabolism suppresses glioma cell proliferation by regulating autophagy, Cell Death Dis. 12 (2021) 1–15.
[42] M. Zöller, CD44: can a cancer-initiating cell profit from an abundantly expressed molecule? Nat. Rev. Cancer 11 (2011) 254–267.
[43] S. Kasai, Y. Furuichi, N. Ando, K. Kagami, K. Goi, T. Inukai, K. Sugita, Triggering of CD44 by ultra-low-molecular-weight hyaluronan induces cell death by autophagy via endoplasmic reticulum stress in acute lymphoblastic leukemia with MLL gene rearrangements, Blood 120 (2012) 1361.
[44] H. Zhang, H. Liu, Z. Xie, J. Du, C. Jin, Hyaluronic acid-functionalized supramolecular nanophotosensitizers for targeted photoimmunotherapy of triple-negative breast cancer, Nanobiotechnol 22 (2024) 777.